



A DFT study to investigate the physical, electrical, optical properties and thermodynamic functions of boron nanoclusters ($M_xB_{2n}^0$; $x=1,2$, $n=3,4,5$)

Milon ^{a,*}, Debashis Roy ^b, Farid Ahmed ^c

^a Department of Physics, Comilla University, Cumilla 3506, Bangladesh

^b Department of Physics, Jashore University of Science and Technology, Jashore, 7408, Bangladesh

^c Department of Physics, Jhangirnagar University, Savar, Dhaka 1342, Bangladesh

ARTICLE INFO

Keywords:

Boron
Nanoclusters
DFT
MEP
Transition metal atoms Doping.

ABSTRACT

First Principle DFT calculations employing the B3LYP/LanL2DZ/SDD level of theory were used to analyze the various characteristics of boron nanoclusters (B_6 , B_8 , and B_{10}). These pure structures were further doped with four transition metals (Ta, Ti, Tc, and V) to examine the enhancement of the pure structures' structural, electrical, and optical features. To study structural stability, we have estimated cohesion energy and imaginary frequencies. Cohesion energies were entirely negative, with a range of -3.37 eV to -8.07 eV, and most constructions had no imaginary frequencies, indicating their structural occurrences. The calculated adsorption energy suggests that the order of stability of the pristine boron nanoclusters is $B_{10} > B_8 > B_6$, and TcB_{10} and Tc_2B_{10} are the more stable structures. Mulliken charge, DOS, HOMO-LUMO, and the HOMO-LUMO gap have all been examined in-depth to provide insight into electrical characteristics. UV-Vis and CD measurements show the doped boron nanoclusters have excellent optical properties. Aside from calculating thermodynamic functions, we have also calculated the global DFT parameters, which give us a deep quantum mechanical understanding of the optimized structure for further research and applications in the field of science and technology.

1. Introduction

Nanostructured materials (zero-dimensional, one-dimensional, two-dimensional, three-dimensional, or bulk nanomaterials) show interesting properties because of their structural morphology and quantum effect [1], which make them promising in technological implementations. Nanostructures, in contrast to bulk materials, have a high aspect ratio, and as a result, have a large number of atoms on the surface of their constituent parts [1–4]. Because these atoms have a purpose that is distinct from that of the atoms located internally, an increase in the number of atoms located on the surface causes a shift in the way that nanostructured materials behave. Getting a cost-effective and reliable energy function-based global minimum nanocluster is a great challenge for researchers [4,5]. Experimental studies on boron nanoclusters have been started after the discovery of fullerenes and have revealed some very interesting properties [6,7], so boron nanoclusters can be one of the favorable choices in this regard.

A large variety of experimental as well as theoretical work has been done on doped and undoped boron nanoclusters to investigate

* Corresponding author.

E-mail addresses: milonpaul@cou.ac.bd (Milon), d.roy@just.edu.bd (D. Roy), fahmed@juniv.edu (F. Ahmed).

their structural, electronic, optical, and magnetic properties in the last decades, as boron nanoclusters show unique properties [8–13]. With exceptional qualities like a lack of electrons, sp^2 orbital hybridizing, a high coordination number, and a small covalent radius, boron is a remarkable element in the periodic table [14]. Possessing a high melting temperature (2300 K), diamond-like hardness [15], and a strong ionizing potential compared to adjacent elements Si and C in the periodic table [16], boron has attractive structural characteristics [17]. Furthermore, as a result of their catenation characteristics that are similar to those of carbon, boron atoms' small covalent radius, and ability to form nanoclusters of various sizes and shapes [14,18]. Boron is capable of forming cage-like crystal structural units as they have an interesting electron deficiency [19,20], but primary studies showed that cage-like boron clusters are not stable enough [14,21–24]. Theoretical studies and photoelectron spectroscopy have been able to characterize the structure and bonding of small boron clusters [7,21–30], which makes the boron nanocluster a significant research element in the scientific domain for utilizing it in technological implementations.

In order to look into the geometries, electronic structures, and energy of the B12 and B13 motifs, Koichi Yamashita and his co-workers [22] optimized a huge number of planar and non-planar stationary structures (neutrals and cations). Anderson and co-workers [24] examined the bonding by measuring the appearance potential and fragmentation pattern in collision-induced dissociation (CID) on boron cluster cations B_{n+2-13} and discovered a distinctive size dependency of various fragmentation channels, as well as the origin of 13 as a magical number. Wang et al. [31–35] showed that the planar and quasi-planar structures are more stable than the other configured structures by exploring the structural stability and chemical bonding among the boron atoms in boron clusters. Where they have performed a theoretical investigation on different clusters of B_n with $n = 1-38$. A systematical study with B3LYP/6-31G* density functional theory has been done by Feng Long Gu et al. [15] on thermodynamically stable B_{12}^+ and B_{13}^+ planar or quasi-planar clusters rather than globular structures. They also experimentally examined the structure and energies of B_{13}^+ cationic boron bunches and computed the dissociation energies of the 3-dimensional B_{13}^+ clusters to compare with the experimental values available. In 2006, a huge work was done by Alexander I. Boldyrev and co-workers [26] on boron planar or quasi-planar nanoclusters (both for neutral and cations). They created a technique known as the ab initio gradient embedded genetic algorithm (GEGA) to obtain the global minimum structure utilizing the semiempirical PM3 approach and the B3LYP/3-21G level of theory for small and large structures, respectively. In order to investigate the geometry and vibrational frequencies of each structure on the Gaussian 03 platform, they additionally employed B3LYP and coupled-cluster CCSD(T) methods with polarized split valence basis sets 6-311 + G.

A significant amount of experimental and theoretical effort has been done to examine the doping effects on nanoclusters over the past decade. Doping or the adsorption of hetero components on any structure can dramatically alter the properties of the pure substances [36–41]. To examine the structural and electronic characteristics of their configured Ta-doped boron clusters B_n ($n = 10-20$), Le Chen, BoSun, Wei Guo Kuang, et al. optimized their tantalum (Ta) doped boron clusters using PBE0 and DFT theory with LanL2DZ and n6-311 + G(d) basis sets in Gaussian 09 platform [42]. In one of our very recent articles, we investigated the B_6 nanocluster for adsorbing heavy metal ions [43]. Recently, U.S.D Shamim and his co-worker investigated the structural, electronic, optical and magnetic properties of intrinsic and Co-doped boron nanocluster B_n ($n = 6-8$) using density functional theory (DFT) at B3LYP level of theory with SDD and LanL2DZ basis sets. Their investigation revealed that the doping of Transition metal atom (TM) enhances stability, and magnetic properties as well as shows fascinating optical properties [44]. To investigate the geometrical structure and electronic properties of Niobium (Nb) doped boron cluster (B_n , $n = 10-16$; 18–20) have been studied by CALYPSO approach tailed by density functional theory and observed noticeable alternation of electronic properties [45]. The investigation of doping of TM (Cr, Mn, Fe, Co, and Ni) in B_n ($n \leq 7$) displayed that CoB_n and NiB_n clusters exhibit fascinating magnetic behavior [46]. A DFT study on Co_2B_6 and Co_2B_7 nanoclusters was performed by Pham and Nguyen to examine the geometry, electronic and structural stability. They found that Co atom doping increased the stability of nanoclusters [47]. From the DFT investigation, J. Wang and his coworker found that the doping of the TM atom in B80 changed the electronic properties interestingly [48].

From the literature review, we found that the TM doped with boron nanocluster enhanced its properties fascinatingly. In our study, we examine the geometrical stability, electrical properties, and optical characteristics of boron nanoclusters with and without TM atom doping. Utilizing the B3LYP/LanL2Z/SDD level of theory, we improved our configured boron nanocluster density functional theory (DFT) on the Gaussian 09 Platform. We have doped the nanoclusters in two distinct ways, referred to as pyramidal and bipyramidal. In a pyramidal manner, just one transition metal was doped, and in a bipyramidal fashion, two transition metals were doped from two opposite sides of the born clusters in a sandwich manner. For the purpose of analyzing the structural, electrical, and optical characteristics of the optimized boron pure and doped nanoclusters, we calculated and examined the cohesion energy, Mulliken charge distribution, dipole moment, HOMO-LUMO, DOS, UV-Vis spectra, CD spectra, MEP, and certain global DFT parameters.

2. Computational details

In this study, we investigated the various properties of three different combinations of neutral boron nanoclusters, consisting of six, eight, and ten boron atoms respectively. Along with we doped these structures with four transition metals (Ta, Tc, Ti, and V) as in the structural formation $M_xB_{2n}^0$ ($x = 1, 2$; $n = 3, 4, 5$; 0 showing the neutrality of the structures). To get a stable and neutral structure of pure and transition metal doped boron nanoclusters with global minima were optimized using Gaussian 09 platform [49]. For getting stable and minimum energy structures we used quantum mechanical density functional theory (DFT) along with B3LYP [50] exchange-correlation function and, SDD [51] and LanL2DZ [52] basis sets. As our structures are not so big, we used these above-mentioned functional and basis sets, and also the cause of using DFT is its accuracy of calculations [53,54]. After getting the ground state energy structures using the above-mentioned theories, we also calculated them using TD-SCF, which gives us the excited energy states of our optimized structure. To get thermodynamic parameters as well as bond frequency we also simulated all the structures using the same level of theory following the orthodox procedure. The subsequent frequency, surface energy, electronic

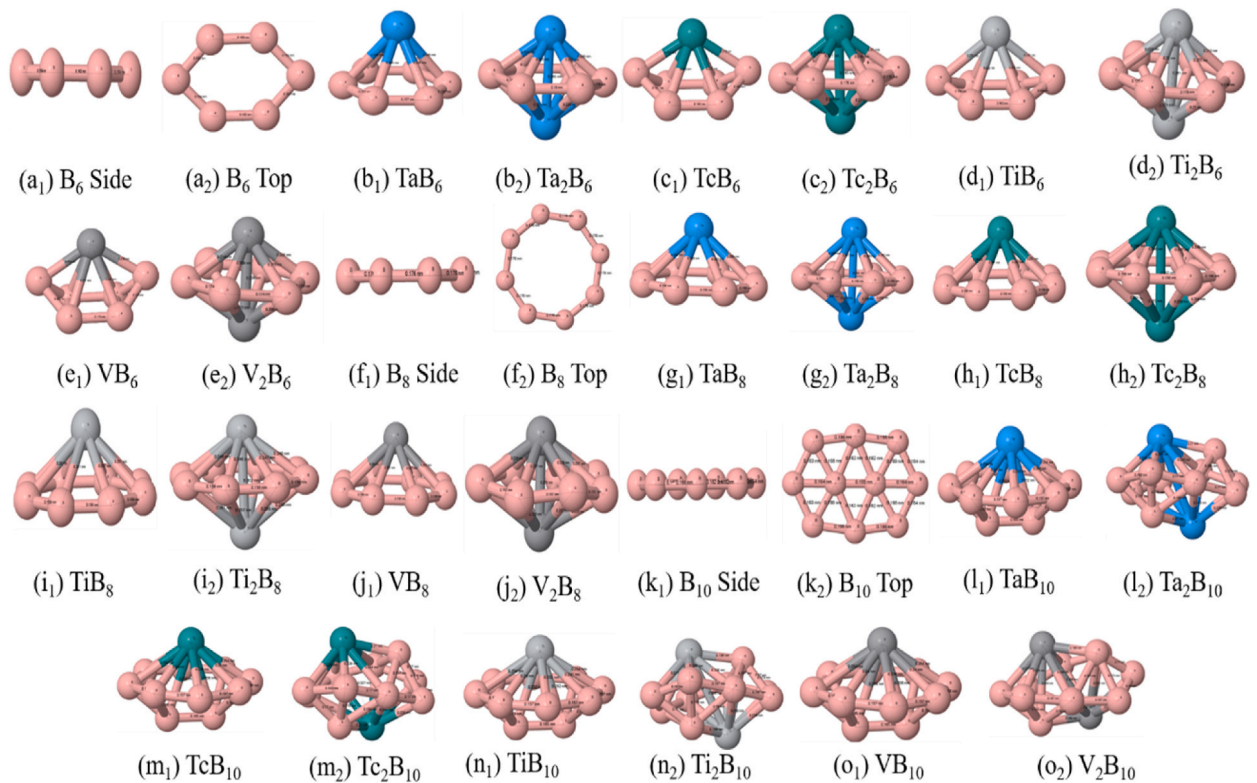


Fig. 1. Optimized global minimum structures of pristine and transition metal (Ta, Tc, Ti, and V) doped B₆, B₈, and B₁₀ nanostructures defined by their chemical definitions.

energies, dipole moments, and partial charge analysis of all compounds were also investigated using the same level of theory [55].

The structural stability of a complex structure, doped by hetero-elements can be explained effectively by analyzing the cohesion energy of that structure. The cohesion energies (E_{co}) per atoms of pure and transition metals doped structures ($M_xB_n^0$) can be calculated using the equations below [56].

$$E_{co} = \frac{1}{N} (E_{com} - nE_B) \quad (1)$$

$$E_{co} = \frac{1}{N} [E_{com} - (nE_B + mE_M)] \quad (2)$$

Where E_{co} represented the cohesion energy of the configured structures. E_{com} , E_B , and E_M represented the energy of complex systems, the energy of each boron atom, and the energy of adsorbed transition metals (Ta, Tc, Ti, and V) respectively. We used n and m in equations (1) and (2) for denoting the number of boron atoms and transition metals correspondingly. And N is defining the total number of atoms in each nanocluster. When atoms or molecules are doped on the surface of a substance, the charge is exchanged between the dopants and substances. In our work, we doped transition metals on a boron nanocluster considering various structural configurations. The charge transfer here is calculated by the varying charge concentration on metal after adsorbing on the surface of the boron nanocluster. The calculation has been done by the Mullikan charge [57] analysis.

The energy stored by chemical elements during bond formation is called chemical potential (μ) and that is calculated by the following equation [58],

$$\mu = -(E_{HOMO} + E_{LUMO}) / 2 \quad (3)$$

Where E_{HOMO} is the energy of the highest occupied molecular orbitals and E_{LUMO} is the energy of the lowest unoccupied molecular orbitals.

To reveal the chemical activity of the configured structures we calculated chemical hardness, chemical softness, and electrophilicity. In calculating the chemical hardness (η) of the structures we have a well-known Koopman's theorem [59]

$$\eta = (E_{LUMO} - E_{HOMO}) / 2 \quad (4)$$

The chemical softness can be obtained by Ref. [52],

Table 1
Tabulated data of Mulliken charge (e), dipole moment μ (Debye), cohesion energy (eV).

Elements	Mulliken charge (e)		Dipole Moment μ (Debye)		Cohesion Energy (eV)	
	Lan	SDD	Lan	SDD	Lan	SDD
B ₆	0.284	0.29	0	0	-3.38	-3.37
TaB ₆	0.579	0.528	4.9515	5.3506	-3.90	-4.04
Ta ₂ B ₆	0.454	0.453	0.0003	0.0007	-4.57	-4.71
TcB ₆	0.325	0.328	2.5653	2.7337	-4.04	-3.94
Tc ₂ B ₆	0.177	0.497	0.0004	1.2337	-4.42	-4.24
TiB ₆	0.672	0.238	5.2678	5.3557	-3.80	-3.80
Ti ₂ B ₆	0.585	0.026	0.0015	0.0032	-4.18	-4.15
VB ₆	0.379	0.093	2.6097	2.6583	-3.72	-3.80
V ₂ B ₆	0.319	0.042	0.0002	0.0012	-4.02	-4.12
B ₈	0.001	0.001	0	0	-3.61	-3.60
TaB ₈	0.517	0.671	4.1895	4.5388	-4.28	-4.36
Ta ₂ B ₈	0.245	0.216	0.0003	0.0014	-4.52	-4.84
TcB ₈	0.19	0.312	3.9347	3.9012	-4.40	-4.34
Tc ₂ B ₈	0.028	0.263	0	0.0004	-4.66	-4.51
TiB ₈	0.742	0.034	3.577	3.7032	-4.09	-4.11
Ti ₂ B ₈	0.436	0.075	0.0014	0.0028	-4.41	-4.42
VB ₈	0.251	0.038	3.4796		-4.09	-4.09
V ₂ B ₈	0.236	0.252	0.0004	0.0007	-4.24	-4.38
B ₁₀	0.38	0.39	0	0	-4.13	-4.12
TaB ₁₀	0.381	0.223	4.3753	4.3853	-2.49	-4.47
Ta ₂ B ₁₀	0.549	0.788	1.8016	1.862	-4.58	-4.67
TcB ₁₀	0.135	0.199	2.1415	2.2065	-6.29	-4.31
Tc ₂ B ₁₀	0.558	0.465	0.8546	0.8609	-8.07	-4.46
TiB ₁₀	0.681	0.243	4.8524	4.8885	-4.94	-4.29
Ti ₂ B ₁₀	0.507	0.777	0.4899	0.5472	-5.58	-4.40
VB ₁₀	0.427	0.422	3.4628	3.4696	-5.18	-4.30
V ₂ B ₁₀	0.265	0.619	1.0276	1.1525	-5.92	-4.31

$$S = 1/2 \eta \quad (5)$$

Electrophilicity (ω) can be calculated by [56]

$$\omega = \mu^2 / 2 \eta \quad (6)$$

For understanding the adsorption process and spontaneous reaction between two substances, the thermodynamic parameters can give a deeper understanding. In this regard we have calculated some major thermodynamic parameters, which are Gibbs free energy ΔG , Enthalpy ΔH , and Entropy ΔS using the same level of theory following the equations below [60]:

$$\Delta G = G_{\text{com}} - (G_B + mG_M) \quad (7)$$

$$\Delta H = H_{\text{com}} - (H_B + mH_M) \quad (8)$$

$$\Delta S = (\Delta H - \Delta G) / T \quad (9)$$

In equation (7) G_{com} represents the Gibbs free energy of the complex structures, G_B for pure boron cluster and G_M for transition metals and m ($=1,2$) represents the number of transition metals. In equation (9), T represents the absolute room temperature.

3. Results and discussions

3.1. Structure and stability

In this ongoing study, we intended to investigate the various promising properties of neutral and transition metal (TM) doped boron nanoclusters for use in a variety of scientific and technological fields. All the lower energy structures were optimized using density functional theory and depicted in Fig. 1(a–o), where the subscripts 1 and 2 represent the top view and side view for pristine structures, and pyramidal and bipyramidal for TM doped structures respectively. In this regard, we constructed three distinct neutral boron nanoclusters with zero charges, each containing a distinct number of boron atoms, denoted by B₆, B₈, and B₁₀. The planar B₆ nanocluster has been configured with six boron atoms that have a central hexagonal vacancy (Fig. 1 (a₂)). On the other hand, B₈ is made up of eight boron atoms and has an octagonal vacancy in the middle. (Fig. 1 (f₂)), and neutral B₁₀ is composed of ten boron atoms that are arranged in a triangular lattice. (Fig. 1 (k₂)). All of the pristine nanoclusters are planar, however following doping with transition metals (Ta, Tc, Ti, and V) in pyramidal and bipyramidal patterns, we observed various structural deformations. To investigate the structural stability of all the 27 boron nanoclusters both pristine and doped, the global minimum structures were optimized by implementing quantum mechanical density functional theory (DFT) with LanL2DZ/B3LYP and SDD/B3LYP level of theory separately. These two levels of

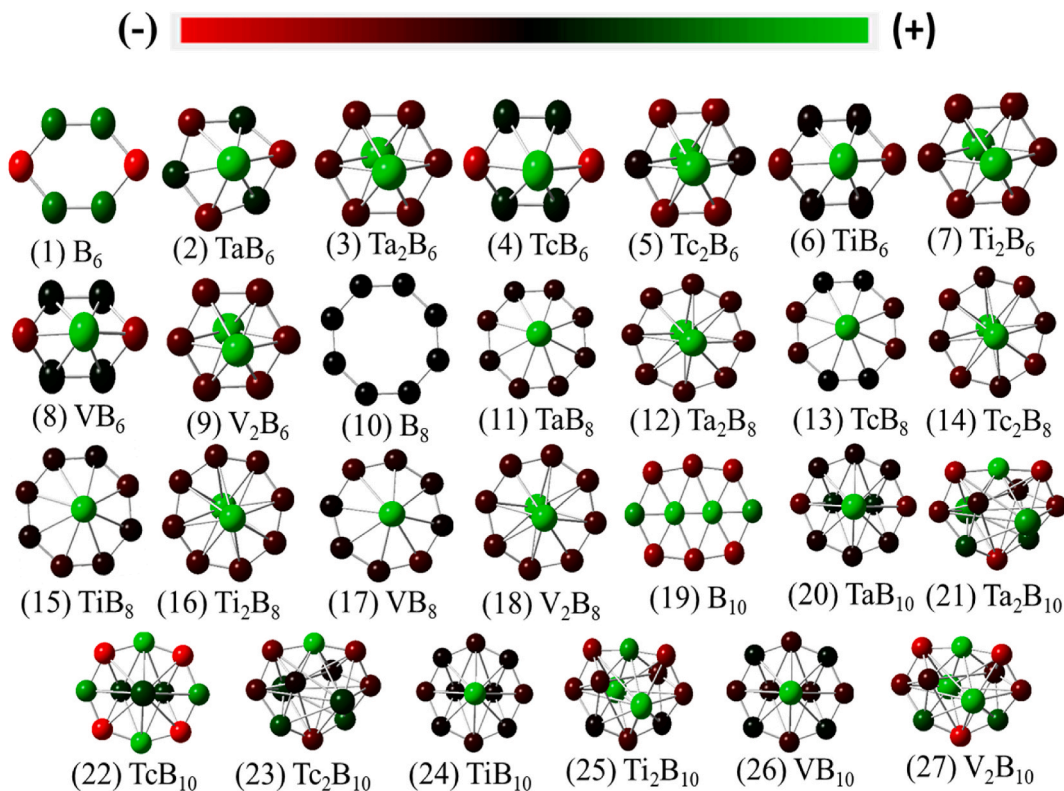


Fig. 2. Color-based Mulliken charge distribution per atom of all the optimized structures. (For interpretation of the references to colour in this figure legend, the reader is referred to the Web version of this article.)

theory give a comparison and impact of the basis set on nanomaterials' optimization. The pristine B_6 nanostructure forms a hexagonal central ring with six boron atoms. The bond length among the boron atoms (B–B) is 1.54 Å and 1.63 Å for corner atoms and top atoms respectively (Fig. 1 (a₂)). But after doping with transition metals (Ta, Tc, Ti, V) the B–B bond lengths in born structures became ranged from 1.57 Å to 1.80 Å depending on the atomic radius, and strength of the bonds of the doped atoms and their connecting boron atoms. We found the bond length for boron atoms in pristine B_8 nanocluster is 1.78 Å, as it forms a perfect octagon. However, after doping, we observed a difference in bond length, and the calculated bond length was 1.56 Å.

It can be seen that for B_6 the lower value and upper value of B–B increased in the case of doped structures but for B_8 it shows a reverse trend; it occurred due to the comparative ring radius of B_6 and B_8 with the doped transition metals. The pristine global minima of neutral B_{10} nanoclusters form a little bit different structure configuration through a triangular lattice instead of forming a ring-like structure as in B_6 and B_8 nanoclusters. Here we found that the B_{10} nanocluster formed a sheet-like structure with a B–B bond length ranging from 1.55 Å to 1.82 Å. Due to doping, there have some structural deformation, (in sheet-to-cage-like structures) which creates B–B bond length variations, and the range of B–B bond length became 1.57 Å to 1.95 Å.

The cohesion energy also called binding energy per atom has been calculated using equations (1) and (2) to give insight into the stability of the optimized nanoclusters. The same level of theories has been used to get the minimum energy structures for calculating cohesion energy. The calculated cohesion energies have been tabulated in Table 1, we see that all the cohesion energies are negative and the span of the cohesion energies starts from –2.49 eV to –8.07 eV per atom. It is also previously reported that a more negative value of cohesion energy indicates more stability in the structures [56]. So, from our calculated data we can write the order of stability of the pristine structures as $B_{10} > B_8 > B_6$. This pattern does not hold in the case of doped structures due to the surface reactivity and nature of the doped atoms.

To get the conformity of the natural existence of our configured structures, we also calculated imaginary frequencies, which gives the other level of conventionality about stability [44]. In the case of calculating imaginary frequencies, we also used the same level of theory. From this calculated date of frequencies, it can be seen that only six structures (B_6 , TcB_8 , B_{10} , TaB_{10} , Tc_2B_{10} , and VB_{10}) show imaginary frequencies among the twenty-seven structures represented in Fig. 1. From the above discussion of cohesion energies and imaginary frequencies, it can be concluded that among the twenty-seven B_n^0 ($n = 6, 8, \text{ and } 10$) nanoclusters twenty-one are stable enough to be considered for further property analysis.

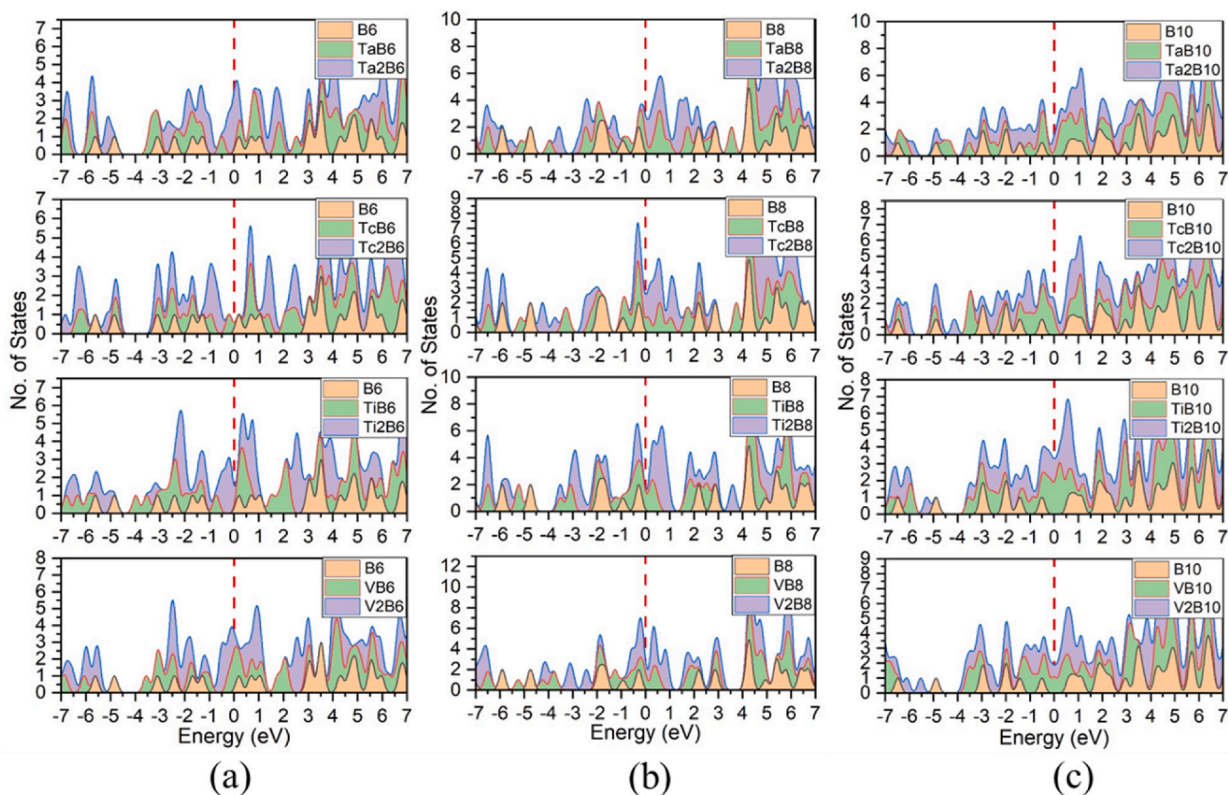


Fig. 3. The Comparative density of state (DOS) spectra of (a) pristine B_6 and its doped structures, (b) pristine B_8 and its doped structures, (c) pristine B_{10} and its doped structures.

3.2. Mulliken charge and dipole moment

The nature of the molecular systems greatly depends on atomic charges and electronegativity of the constituents' atoms. As a result, in quantum chemical computations molecular charge analysis keeps a prodigious effect. Here the charge distribution we have calculated considering Mulliken charge per atom, and the numerical value of net electron charges are represented in Table 1. In Fig. 2 we have shown charge per atom by colour grading, in order of positive to negative by green to red colour. From Fig. 2 it is seen that in the case of pure structures some of the boron atoms carry positive charges (green colour) and some of the atoms carry negative charges (red colour), which make the structures through atomic bonding. The electronegativity of an atom in a structure determines whether that atom has functioned as a donor or acceptor [46]. Here we see that in all the doped structures the adatoms (transition metals) carry positive charges and boron atoms carry negative charges, as the electronegativity of boron atoms is greater than transition metals (Ta, Tc, Ti, and V). In the case of doped structures, the relatively higher electronegativity of boron atoms drew the partial negative charge towards itself, causing it to become a negative charge acceptor in comparison to transition metals, and vice versa. It has been claimed that an atom can more easily donate an electron to an empty orbital of a metal if the atomic charges it carries are more negative [61]. So, from the immediate above lines we conclude that boron atoms will act as a donor and dopant transition metals will act as an acceptor respectively in case of nonbonding interaction with metal and nonmetal contained complexes, like in detecting some toxic molecules.

Bonds are created in molecular systems via the charge transfer mechanism, which results in the formation of a bond dipole moment (BDM), also known as an electric dipole moment (EDM) and indicated by μ_d [62]. In any molecular system, a uniform charge distribution produces a zero-dipole moment, while a nonuniform charge distribution produces a dipole moment in some values. Thus, dipole moment (DM) describes a structure's polarity. The DMs are ranges from 0 to 11 Debye for single-bonded structures, but for many bonded structures the μ_d is the vector sum of the dipole moment of individual bonds [63]. The calculated DMs for our structures are tabulated in Table 1 and obtained by using the dedicated Gauss view tool in Gaussian 09. The tabulated DMs for pure boron clusters are zero, indicating that there is no polarity in pure boron nanoclusters. However, after doping with transition metals, we obtain some value of μ_d , and it is also observable that pyramidal structures exhibit greater dipole moments than bipyramidal doped structures. All the bipyramidal doped structures have a very little amount of dipole moment as the Mulliken charges distribution in bipyramidal structures is nearly uniform, but for pyramidal doped structures, the charge distribution is not uniform, which produces a large dipole moment.

Table 2
HOMO-LUMO, Fermi level, and electronic band gap.

Elements	HOMO (eV)		LUMO (eV)		HOMO-LUMO gap (eV)	
	Lan	SDD	Lan	SDD	Lan	SDD
B ₆	-5.61	-5.61	-4.84	-4.84	0.77	0.77
TaB ₆	-5.77	-6.05	-3.85	-4.00	1.92	2.05
Ta ₂ B ₆	-5.11	-5.05	-2.75	-2.74	2.36	2.31
TcB ₆	-6.07	-6.10	-3.82	-3.78	2.25	2.32
Tc ₂ B ₆	-4.74	-5.11	-3.16	-3.14	1.58	1.97
TiB ₆	-5.89	-5.86	-3.97	-3.82	1.92	2.03
Ti ₂ B ₆	-5.09	-4.91	-3.25	-3.08	1.83	1.83
VB ₆	-6.06	-6.08	-3.93	-3.86	2.14	2.21
V ₂ B ₆	-5.50	-5.36	-2.56	-2.50	2.94	2.86
B ₈	-5.90	-5.90	-4.74	-4.73	1.17	1.17
TaB ₈	-6.48	-6.46	-4.89	-4.99	1.59	1.47
Ta ₂ B ₈	-5.53	-5.43	-3.57	-3.49	1.43	1.93
TcB ₈	-6.41	-6.44	-4.98	-5.02	1.43	1.42
Tc ₂ B ₈	-5.87	-5.99	-4.24	-4.33	1.63	1.66
TiB ₈	-6.49	-6.43	-5.17	-4.99	1.32	1.45
Ti ₂ B ₈	-5.65	-5.44	-3.52	-3.43	2.13	2.01
VB ₈	-6.43	-6.06	-4.06	-3.32	2.37	2.73
V ₂ B ₈	-6.59	-6.55	-4.11	-3.90	2.48	2.65
B ₁₀	-6.48	-6.47	-4.89	-4.88	1.59	1.59
TaB ₁₀	-5.65	-5.61	-3.72	-3.68	1.92	1.93
Ta ₂ B ₁₀	-4.89	-4.84	-3.60	-3.56	1.29	1.28
TcB ₁₀	-5.46	-5.86	-3.70	-4.58	1.76	1.28
Tc ₂ B ₁₀	-5.75	-5.76	-3.74	-3.72	2.01	2.05
TiB ₁₀	-5.90	-5.85	-3.53	-3.46	2.37	2.39
Ti ₂ B ₁₀	-5.28	-5.21	-3.42	-3.36	1.86	1.86
VB ₁₀	-6.73	-6.61	-3.39	-3.36	3.33	3.24
V ₂ B ₁₀	-5.52	-5.46	-3.69	-3.61	1.83	1.84

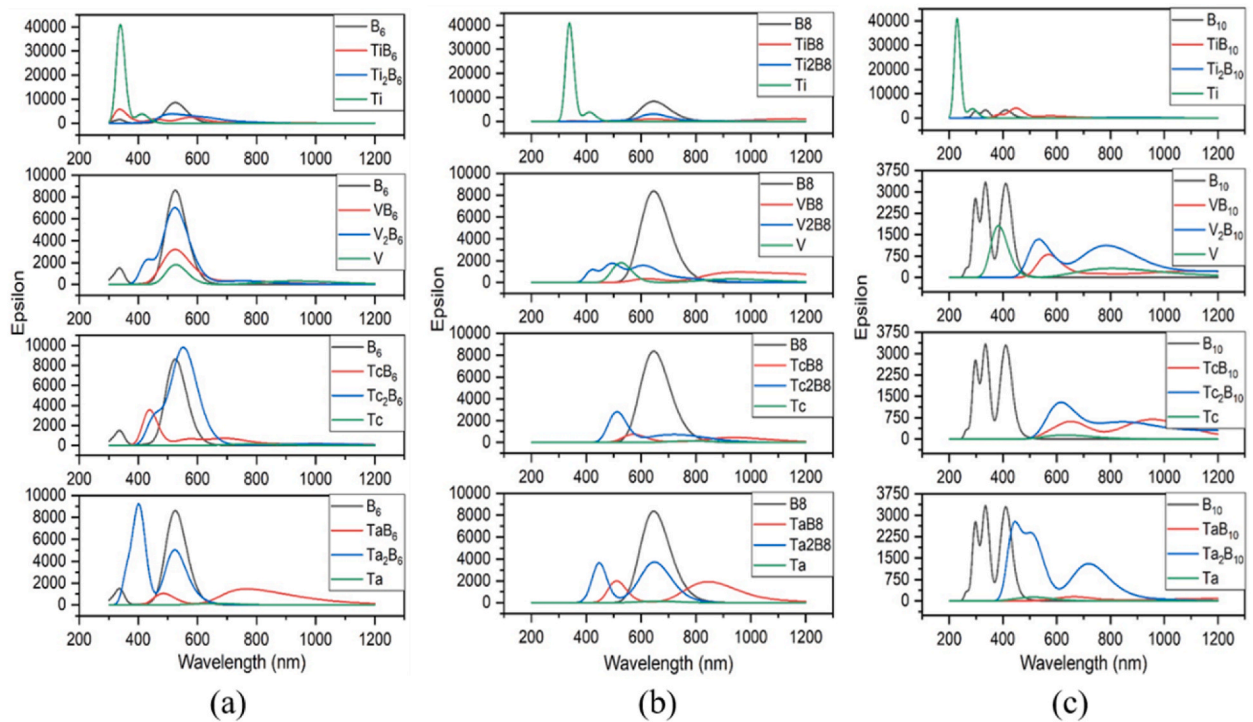


Fig. 4. Comparative UV-Vis spectra (a) pristine B₆ and its doped structures (b) pristine B₈ and its doped structures (c) pristine B₁₀ and its doped structures.

3.3. Frontier molecular orbital and DOS spectra analysis

Fig. 3(a–c) are the representation of the density of state (DOS) spectra, and red dotted vertical lines at zero positions on each graph is indicating the Fermi level. At absolute zero temperature, the Fermi level in a chemical system defines the chance of finding electrons above the valance. The numerical values of the HOMO, LUMO, and HOMO-LUMO gap (E_g) are represented in Table 2. The pristine boron nanostructures have a lower HOMO-LUMO gap than the doped structures, it is also noticeable that the bipyramidal doped structures have a lower HOMO-LUMO gap than the pyramidal doped structures except few anomalies, this result may come out due to the metal-metal interaction in bipyramidal doped structures. As the HOMO-LUMO gap increased the structure will be less reactive, that is the stability of the structure is increased, which justifies the calculated cohesion energies of the pristine and doped structures.

The pristine B_6 nanostructures have a value of E_g is 0.77 eV, which is the semiconducting range, but the HOMO-LUMO gap raised to 2.94 eV for transition metals doped boron nanostructures which are also semiconducting range, it is occurred due to the shifting of HOMO and LUMO peak from and to the Fermi level, that we can confirm from the DOS spectra (Fig. 3). As we see that the E_g (s) for most of the doped structures are comparable to the 1.5 eV photon energy, so they can be used in photo voltaic applications. From the tabulated data of E_g , we can make an order of HOMO-LUMO gap for doped B_6 as $V_2B_6 > Ta_2B_6 > TcB_6 > VB_6 > TaB_6 > TiB_6 > Ti_2B_6 > Tc_2B_6 > B_6$.

In the case of pristine B_8 , we found the HOMO-LUMO gap of 1.17 eV, but after doping by transition metals the gaps are increased up to 2.48 eV, these are also comparable to maximum photon flux. These variations in the HOMO-LUMO gap are caused by the shifting of the HOMO and LUMO peaks away from and towards the Fermi level, as depicted graphically in Fig. 3. According to the tabulated data of E_g s, we can have the order as $V_2B_8 > VB_8 > Ti_2B_8 > Tc_2B_8 > TaB_8 > Ta_2B_8 > TcB_8 > TiB_8 > B_8$.

After being doped, the sheet-like structure of neutral B_{10} transforms into a case-like structure. The calculated HOMO-LUMO gap of pristine B_{10} is 1.59 eV, which is the maximum visible absorbing range of visible photon, but after doping the HOMO and LUMO peak shift a little bit, which changes the E_g value of doped B_{10} nanoclusters (Table 2). The order of the HOMO-LUMO gap of B_{10} nanoclusters are as follows $VB_{10} > TiB_{10} > Tc_2B_{10} > TaB_{10} > Ti_2B_{10} > V_2B_{10} > TcB_{10} > B_{10} > Ta_2B_{10}$. From the discussion of DOS and HOMO-LUMO, it is revealed that doping has a great effect on DOS and HOMO-LUMO, i.e., the electrical properties of boron nanoclusters.

3.4. Absorption spectra

Fig. 4(a–c) illustrates the comparative absorption (UV–Vis) spectra of pure, pyramidal, and bipyramidal doped boron nanoclusters, where the black graph represents pure structures (B_6 , B_8 , and B_{10}), green represents doped atoms (Ti, V, Tc, and Ta), and red and blue representing pyramidal and bipyramidal doped structures, respectively. We optimized all the formations using time-dependent density functional theory (TD-DFT) to get absorption spectra.

From Fig. 4 (a) the comparative representation of absorption spectra of B_6 and their doped complexes, we see that the pure B_6 covers the absorption range nearly from 450 nm to 630 nm with the maximum transition energy of 1.97 eV, and after doping by Titanium (Ti) atom it becomes wider for both the pyramidal and bipyramidal doping manner. And the covering range of absorption becomes 300 nm–700 nm and 450 nm–700 nm respectively for pyramidal and bipyramidal doped structures. For vanadium (V) doped structure it becomes 440 nm–450 nm and 380 nm–450 nm, for Technetium (Tc) doped boron nanostructures it becomes 390 nm–850 nm and 390 nm–770 nm and for Tantalum (Ta) doped B_6 complex we get the shift as 450 nm–1100 nm and 120 nm–650 nm.

Fig. 4 (b) shows the comparative absorption spectra for pristine and doped B_8 nanoclusters, where the representation is the same, discuss in the previous paragraph. Here, it can be seen that the pristine B_8 nanocluster covers the absorption range from 550 nm to 800 nm with the maximum electron transition energy of 1.55 eV, but transition metal doping shows a change of wavelength in absorption spectra. The Ti has little contribution to absorption spectra and makes the range narrower for both pyramidal and bipyramidal doped B_8 nanostructures, and the range is 570 nm–720 nm and 570 nm–750 nm.

For the V-doped structure, we see some good effects of doping on UV–Vis spectra, where we see that the absorption wavelength becomes greater the 530 nm and 390 nm–850 nm correspondingly for single and double-doped structures. We get the absorption range greater the 500 nm and 430 nm–900 nm for Tc-doped pyramidal and bipyramidal structures respectively. In the case of Ta-doped structures, they become 450 nm–1200 nm and 390 nm–800 nm respectively for pyramidal and bipyramidal doped B_8 nanocluster. In Fig. 4 (c) we represented the comparative UV–Vis spectrum for pure and transition metal doped B_{10} nanoclusters in the same way we represented in the case of B_6 and B_8 nanoclusters. From the figure, it is seen that the pure B_{10} covers the absorption wavelength range 250 nm–500 nm, which is a partially ultraviolet and partially visible range, but after doping by transition metals we see a redshift, which covers the visible to UV range. For Ti-doped structures we see a small red shift compared to other transition metal-doped structures, the range of absorption wavelength 350 nm–460 nm for TiB_{10} (pyramidal), but for Ti_2B_{10} (bipyramidal) we do not see any absorption peak at all. In the case of the rest three structures large redshifts occurred. For VB_{10} the absorption wavelength covers the range 500 nm–700 nm and for V_2B_{10} we have the range 450 nm–1100 nm. The Tc-doped pyramidal structure covers the range 500 nm–1200 nm and the bipyramidal structure shows a covering range of more than 500 nm. In the case of the TaB_{10} nanosheet, the absorption peak is negligibly small, but V_2B_{10} covers a large range from visible to near UV (400 nm–950 nm).

From the above comparative argument of UV–Vis spectra of all the optimized structures, it can be concluded that most of the structures absorb visible range light and very little ultraviolet or infrared. As the pure and doped boron nanoclusters are optically active, can be used in nonlinear optical (NLO) applications, in the medical field, UV sensors, and so on.

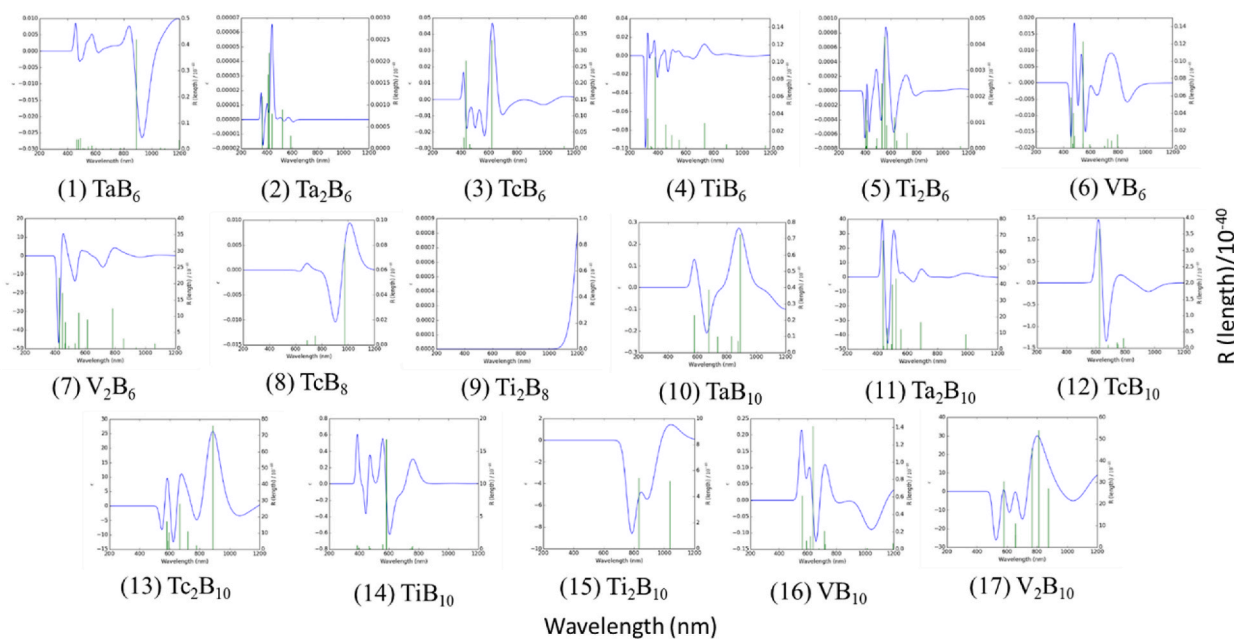


Fig. 5. Circular dichroism (CD) spectra of the configured optimized structures with their chemical formula.

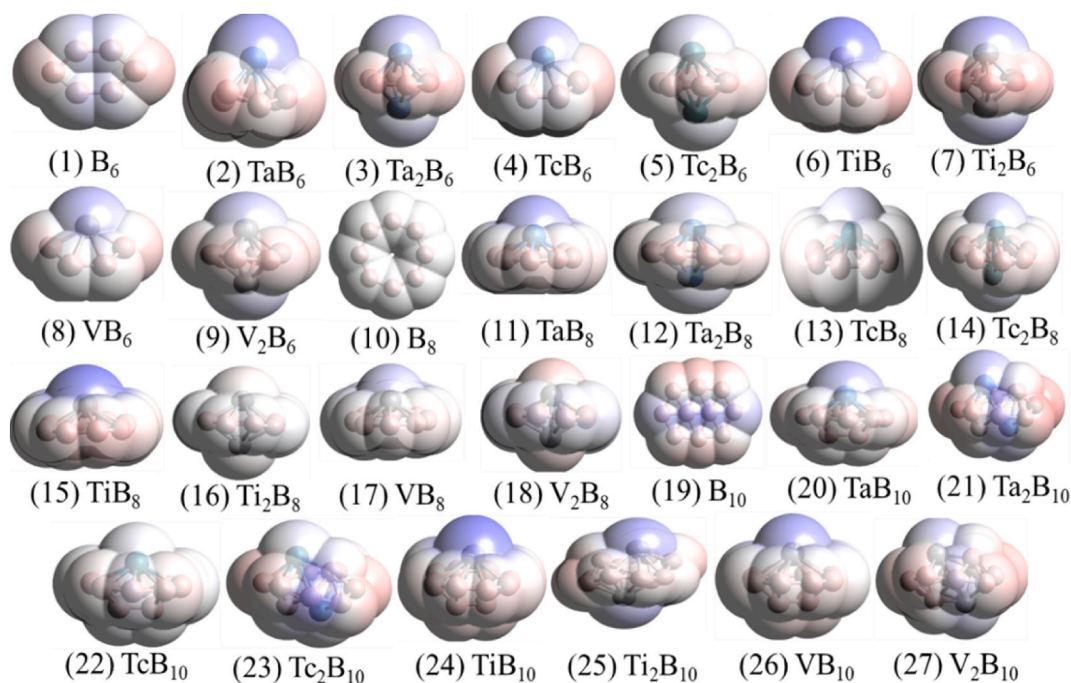


Fig. 6. Molecular electrostatic potential (MEP) of all the configured twenty-seven structures.

3.5. Circular dichroism (CD)

Circular Dichroism (CD) is a spectroscopic technique based on the differential absorption of left and right circularly polarized light [64]. Optically active chiral molecules will preferentially absorb one direction of the circularly polarized light. During the transmission of circularly polarized light inside optically active materials, the two states of photon spin angular momentum are described by right-handed or left-handed CD spectra [43,65]. The existence of CD spectra of a molecular system indicates that the molecular system has chirality and it is optically active i.e., rotation of the plane of polarization occurs when a plane of polarized light travels through the

Table 3
Global DFT parameters: chemical hardness, chemical softness, and electrophilicity.

Elements	HOMO-LUMO Gap Eg (eV)		Chemical hardness η (eV)		Chemical Softness S (eV) ⁻¹		Electrophilicity ω (eV)		Chemical Potential μ eV	
	Lan	SDD	Lan	SDD	Lan	SDD	Lan	SDD	Lan	SDD
B ₆	0.77	0.77	0.3873	0.3867	1.2909	1.2931	5.29	5.27	-5.23	-5.22
TaB ₆	1.92	2.05	0.9592	1.0236	0.5213	0.4885	11.11	12.93	-4.81	-5.03
Ta ₂ B ₆	2.36	2.31	1.1800	1.1551	0.4237	0.4329	9.11	8.78	-3.93	-3.90
TcB ₆	2.25	2.32	1.1234	1.1616	0.4451	0.4304	13.72	14.17	-4.94	-4.94
Tc ₂ B ₆	1.58	1.97	0.7911	0.9843	0.6320	0.5080	6.16	8.37	-3.95	-4.12
TiB ₆	1.92	2.03	0.9616	1.0174	0.5200	0.4915	11.69	11.91	-4.93	-4.84
Ti ₂ B ₆	1.83	1.83	0.9162	0.9136	0.5458	0.5473	7.97	7.30	-4.17	-4.00
VB ₆	2.14	2.21	1.0683	1.1061	0.4680	0.4520	13.33	13.66	-4.99	-4.97
V ₂ B ₆	2.94	2.86	1.4708	1.4292	0.3399	0.3498	11.92	11.03	-4.03	-3.93
B ₈	1.17	1.17	0.5841	0.5839	0.8561	0.8563	8.26	8.24	-5.32	-5.31
TaB ₈	1.59	1.47	0.7962	0.7390	0.6280	0.6766	12.87	12.11	-5.69	-5.73
Ta ₂ B ₈	1.43	1.93	0.9830	0.9675	0.5087	0.5168	10.17	9.62	-4.55	-4.46
TcB ₈	1.43	1.42	0.7154	0.7100	0.6990	0.7042	11.59	11.65	-5.69	-5.73
Tc ₂ B ₈	1.63	1.66	0.8139	0.8302	0.6143	0.6023	10.39	11.05	-5.05	-5.16
TiB ₈	1.32	1.45	0.6611	0.7242	0.7564	0.6904	11.22	11.80	-5.83	-5.71
Ti ₂ B ₈	2.13	2.01	1.0646	1.0065	0.4697	0.4968	11.19	9.91	-4.58	-4.44
VB ₈	2.37	2.73	1.1846	1.3661	0.4221	0.3660	16.31	15.02	-5.25	-4.69
V ₂ B ₈	2.48	2.65	1.2419	1.3254	0.4026	0.3772	17.79	18.08	-5.35	-5.22
B ₁₀	1.59	1.59	0.7947	0.7951	0.6292	0.6289	12.82	12.79	-5.68	-5.67
TaB ₁₀	1.92	1.93	0.9621	0.9669	0.5197	0.5171	10.56	10.43	-4.68	-4.65
Ta ₂ B ₁₀	1.29	1.28	0.6475	0.6405	0.7722	0.7806	5.83	5.65	-4.25	-4.20
TcB ₁₀	1.76	1.28	0.8778	0.6385	0.5696	0.7831	9.21	8.70	-4.58	-5.22
Tc ₂ B ₁₀	2.01	2.05	1.0031	1.0227	0.4985	0.4889	11.28	11.49	-4.74	-4.74
TiB ₁₀	2.37	2.39	1.1842	1.1929	0.4222	0.4192	13.15	12.91	-4.71	-4.65
Ti ₂ B ₁₀	1.86	1.86	0.9302	0.9276	0.5375	0.5390	8.78	8.51	-4.35	-4.28
VB ₁₀	3.33	3.24	1.6668	1.6208	0.3000	0.3085	21.32	20.14	-5.06	-4.99
V ₂ B ₁₀	1.83	1.84	0.9155	0.9232	0.5462	0.5416	9.72	9.48	-4.61	-4.53

systems [66].

We have a total of twenty-seven optimized structures including the pristine and transition metals doped boron nanoclusters, shown in Fig. 5, and these spectra are obtained from the output file of Gaussian calculations by using the *Gauss-sum tool*. Among the total twenty-seven structures, seventeen structures show CD spectra. We also find that none of the pure boron nanoclusters has CD, which suggests that the pristine structures have no chirality and optical activity on circularly polarized lights. On the other hand, the doped structures show CD spectra except for Tc₂B₆, TaB₈, Ta₂B₈, Tc₂B₈, TiB₈, VB₈, and V₂B₈. The CD analysis of the boron nanoclusters recommends that most of the doped structures are optically active to circularly polarized light and have the maximum CD peak at the visible range or near UV range (Fig. 5) and have wide application in medical experiments [67,68]. Thus, we can conclude that doped boron nanoclusters enhance their optical activity by doping transition metals.

3.6. MEP maps

The MEP is a plot of the electrostatic potential on a surface with a constant number of electrons. We have calculated MEP to understand the reactivity of our structures by using the same level of the theory mentioned above and represented in Fig. 6 (1-27). Since an electrophile will be drawn to a negative charge, the MEP is a useful property to study reactivity. Most MEPs have a red colour for the area with the most negative charge, which is where electrophilic attacks tend to happen, and a blue colour for the area with the most positive charge, which is where nucleophilic attacks tend to happen. MEP is important because it uses colour to show the size, shape, positive, negative, and neutral electrostatic potential regions of molecules at the same time [69–71]. This makes it a very useful tool for studying the relationship between the structure of molecules and their physical and chemical properties. The resultant surface reflects the size and shape of molecules as well as their electrostatic potential value. Here in our research, the order of the positive to the negative surface is blue-white-red, with white representing the neutral surface area and blue and red representing the positive and negative regions respectively.

Here, we observe that the pure structures (B₆, B₈, and B₁₀) exhibit a light blue colour in the positive area of certain boron atoms in boron clusters and a faint red colour in the negative region of the remaining boron atoms. In contrast, in doped structures, the transition metals (Ta, Tc, Ti, and V) seem a little bit deep blue for positive reasons, except for a few oddities. We may also see that the colour gradation, form, and size of the MEP for various structures are distinct because the kind and electronic nature of the individual atoms are distinct.

3.7. Physical parameters and chemical potential

Three physical parameters also called global DFT parameters are hardness (η), softness (S), and electrophilicity (ω) are calculated using equations from (4) (5), and (6), and data are tabulated in Table 3. The tabulated physical parameters are following a correlation

Table 4
Thermodynamic parameters Gibbs free energy, Enthalpy, and Entropy.

Elements	Gibbs Free Energy (eV)		Enthalpy (eV)		Entropy (eV/K)	
	Lan	SDD	Lan	SDD	Lan	SDD
TaB ₆	-6.64	-7.69	-7.00	-8.06	-0.00119563	-0.00124354
Ta ₂ B ₆	-15.35	-16.56	-16.19	-17.41	-0.00282768	-0.00284155
TcB ₆	-7.25	-6.57	-7.61	-6.95	-0.00119791	-0.00125751
Tc ₂ B ₆	-14.29	-12.89	-15.11	-13.66	-0.00274464	-0.00258575
TiB ₆	-5.93	-5.94	-6.31	-6.29	-0.00128106	-0.00116442
Ti ₂ B ₆	-12.33	-12.15	-13.11	-12.93	-0.00262855	-0.00262326
VB ₆	-5.42	-5.93	-5.77	-6.28	-0.00116698	-0.00118605
V ₂ B ₆	-10.98	-11.87	-11.77	-12.67	-0.00266798	-0.00268422
TaB ₈	-9.12	-10.01	-9.64	-10.46	-0.00175006	-0.00150994
Ta ₂ B ₈	-15.36	-16.60	-16.24	-17.52	-0.00295409	-0.00309335
TcB ₈	-9.57	-9.15	-10.09	-9.67	-0.00175279	-0.00172578
Tc ₂ B ₈	-16.75	-15.33	-17.70	-16.28	-0.00319027	-0.00318671
TiB ₈	-7.53	-7.76	-8.02	-8.23	-0.0016521	-0.00156698
Ti ₂ B ₈	-14.32	-14.47	-15.17	-15.35	-0.00285379	-0.00294879
VB ₈	-7.09	-7.86	-7.55	-8.34	-0.00155585	-0.00160093
V ₂ B ₈	-12.53	-13.92	-13.48	14.89	-0.0031872	-0.00324941
TaB ₁₀	-6.04	-6.88	-6.34	-7.16	-0.00099522	-0.00094786
Ta ₂ B ₁₀	-12.81	-14.06	-13.62	-14.87	-0.0027138	-0.00273725
TcB ₁₀	-6.94	-6.69	-7.28	-6.96	-0.00114152	-0.00091336
Tc ₂ B ₁₀	-11.04	-9.66	-11.88	-10.50	-0.00281464	-0.00281692
TiB ₁₀	-5.67	-5.72	-5.95	-6.01	-0.00093572	-0.00095160
Ti ₂ B ₁₀	-10.89	-10.81	-11.66	-11.58	-0.00258703	-0.00259725
VB ₁₀	-5.19	-5.79	-5.50	-6.11	-0.00103684	-0.00107042
V ₂ B ₁₀	-8.59	-9.71	-9.39	-10.51	-0.00268039	-0.00270028

with the HOMO-LUMO gap. The HOMO-LUMO gap of pristine B₆, B₈, and B₁₀ are 0.77 eV, 1.17 eV, and 1.59 eV respectively, but after doping the E_gs are increased for all of the doped boron nanostructures. We see from the data in Table 3 that the hardness (η) is increased with the increasing nature of the HOMO-LUMO gap, where softness (s) show the reverse nature.

Chemical potential is another popular term in the thermodynamic field, it is also known as partial molar free energy, defined as the required energy which is needed during a chemical reaction or phase transition, in semiconductor physics it is termed as Fermi level energy [72]. To calculate the value of chemical potential energy we used equation (3). The calculated value of chemical potential (μ) of pure B₆, B₈, and B₁₀ are -5.23 eV, -5.32 eV, and -5.68 eV, but the values of chemical potential varied noticeably for doped structures. It is also noticeable that the calculated value of μ for pyramidal and bipyramidal doped structures shows a trend, bipyramidal doped structures carry a smaller value of μ compared to pyramidal doped structures, which may happen due to the metal-metal interaction in bipyramidal structures.

Electrophilicity (ω) is a term that is highly dependent on the chemical potential (μ) and the hardness (η) of a system to define its affinity for electrons. The values tabulated in Table 3 for electrophilicity (ω) are calculated by equation (6). Based on the tabular values of (μ), (ω), and (η), it can result that the value of ω increases as the chemical potential increases and decreases as the hardness increases.

3.8. Thermodynamic parameters

Calculations of thermodynamic parameters are critical for observing the doping stability of the constructed structures. We estimated thermodynamic parameters using the previously specified level of theory to better explain the doping phenomena and calculated the thermodynamical values using equations (7)–(9). The thermodynamic parameters for pyramidal and bipyramidal transition metals doped B₆, B₈, and B₁₀ nanoclusters are shown in Table 4. The Gibbs free energies and enthalpies are tabulated in Table 4, and we discovered that the metal-doped bipyramidal structures have a higher negative value of free energies. The amount of mechanical work that a system can do is defined by its free energy. The higher the negative value of free energy, the more spontaneous adsorption of doped atoms on a substrate surface occurs, and our calculated findings match the measurements [73,74]. The calculated enthalpy values of the optimized structures are also large negative values, more than 1eV, which means structures are formed through the chemical adsorption process. The estimated values of enthalpy are very small negative, which indicates that the structures are orderly enough. The discussion of thermodynamic parameters advocates that our optimized structures are stable and ordered enough to apply in different compatible fields in science and technology.

4. Conclusion

We performed here a computational study using DFT using B3LYP/LanL2DZ/SDD level of theory to investigate the various properties of boron nanoclusters (B₆, B₈, and B₁₀). We also doped these pure structures with four transition metals (Ta, Ti, Tc, and V) to study the structural, electrical, and optical properties enhancement of the pure structures. In this respect, we have calculated cohesion energy and imaginary frequencies to investigate structural stability and natural existence respectively. We got all the cohesion energy

negative and most of the structures have no imaginary frequencies, which revealed their structural stability. According to the computed adsorption energy we are capable to make a trend of stability of pure structures as $B_{10} > B_8 > B_6$ also found TcB_{10} and Tc_2B_{10} are the more stable structures since they have larger negative adsorption energy values. To investigate electrical properties, we have analyzed Mulliken charge, DOS, HOMO-LUMO, and HOMO-LUMO gap, which suggests that after doping large changes in HOMO-LUMO gap created because of orbital hybridization between the dopants and substrates elements. Absorption spectra (UV-Vis) and circular dichroism (CD) analysis result in good optical properties of the doped boron nanoclusters, as we found considerable shifting of absorption peak in the absorption spectra furthermore, we also got some CD spectra for doped structures that were absent in pure clusters. In addition, we have also calculated some thermodynamic parameters (Gibbs free energy, Enthalpy, and entropy) and global DFT parameters (chemical hardness, chemical softness, and electrophilicity). The quantum mechanical insight into the optimized structure gained through these computations will be useful for future scientific and technological advancement.

Author contribution statement

Milon: Conceived and designed the experiments; Performed the experiments; Analyzed and interpreted the data; Wrote the paper.
 Debashis Roy: Conceived and designed the experiments; Analyzed and interpreted the data; Wrote the paper.
 Farid Ahmed: Contributed reagents, materials, analysis tools or data; Wrote the paper.

Data availability statement

Data included in article/supplementary material/referenced in article.

Declaration of competing interest

The authors declare that they have no known competing financial interests or personal relationships that could have appeared to influence the work reported in this paper.

Acknowledgment

Comilla University (CoU) and the University Grant Commission (UGC) of Bangladesh are thanked for the financial support that allowed us to purchase the essential software and perform the study.

References

- [1] A. Alagarasi, Chapter - introduction to nanomaterials, Nat. Cent. Catal. Res., (November) (2011) 1, <https://doi.org/10.1002/9781118148419.-23>.
- [2] C.N.R. Rao, A. Müller, A.K. Cheetham, Nanomaterials - an introduction, in: *The Chemistry of Nanomaterials*, 2005, pp. 1–11.
- [3] F. Hadeef, *An Introduction to Nanomaterials*, 2018, pp. 1–58.
- [4] J.N. Lalena, D.A. Cleary, An introduction to nanomaterials, in: *Principles of Inorganic Materials Design*, 2010, pp. 531–558.
- [5] S.M. Woodley, S.T. Bromley, Introduction to modeling nanoclusters and nanoparticles, *Front. Nanosci.* 12 (2018) 1–54.
- [6] L. Hanley, S.L. Anderson, Production and Collision-Induced Dissociation of Small Boron Cluster Ions, no. 8, 1987, pp. 5161–5163.
- [7] P.A. Hintz, S.A. Ruatta, S.L. Anderson, P.A. Hintz, S.A. Ruatta, S.L. Anderson, Interaction of boron cluster ions with water : single collision dynamics and sequential etching Interaction of boron cluster ions with water, *Single Coll. Dynam. Seq. Etch.* 292 (1990) (2014), <https://doi.org/10.1063/1.458571>.
- [8] Z. Yang, S.J. Xiong, Structures and electronic properties of small FeBn (n=1-10) clusters, *J. Chem. Phys.* 128 (18) (2008), <https://doi.org/10.1063/1.2913172>.
- [9] T.B. Tai, M.T. Nguyen, Thermochemical properties, electronic structure and bonding of mixed lithium boron clusters (BnLi, n = 1-8) and their anions, *Chem. Phys.* 375 (1) (2010) 35–45, <https://doi.org/10.1016/j.chemphys.2010.07.015>.
- [10] W.L. Li, L. Xie, T. Jian, C. Romanescu, X. Huang, L.S. Wang, Hexagonal bipyramidal [Ta2B6]-10 clusters: B6 rings as structural motifs, *Angew. Chem - Int. Ed.* 53 (5) (2014) 1288–1292, <https://doi.org/10.1002/anie.201309469>.
- [11] L.N. Zhang, J. Jia, H.S. Wu, Structural and electronic properties of V2Bn (n = 1-10) clusters, *Chem. Phys.* 459 (2015) 131–136, <https://doi.org/10.1016/j.chemphys.2015.08.013>.
- [12] M. Yousofzadeh, E. Shakerzadeh, M. Bamdad, Electronic and nonlinear optical characteristics of the LiBn (n = 4–11) nanoclusters: a theoretical study, *Microelectron. Eng.* 183–184 (2017) 64–68, <https://doi.org/10.1016/j.mee.2017.10.011>.
- [13] A.Q. Hao, B.Z. Xu, J. Jia, An insight into the structures, stabilities and magnetic properties of Fe2Bn (n = 1–10) clusters, *Mater. Chem. Phys.* 205 (2018) 1–8, <https://doi.org/10.1016/j.matchemphys.2017.10.066>.
- [14] C. L. S. Y. X. C. H. M. Wang Haiyan, Research advances of boron clusters, borane and metal-doped boron compounds, *Prog. Chem.* 28 (11) (2016) 1601–1614, <https://doi.org/10.7536/PC160533>.
- [15] X.J. Feng, Y.H. Luo, Structure and stability of Al-doped boron clusters by the density-functional theory, *J. Phys. Chem. A* 111 (12) (2007) 2420–2425, <https://doi.org/10.1021/jp0656429>.
- [16] J.G. Yao, X.W. Wang, Y.X. Wang, A theoretical study on structural and electronic properties of Zr-doped B clusters: ZrBn (n = 1-12), *Chem. Phys.* 351 (1–3) (2008) 1–6, <https://doi.org/10.1016/j.chemphys.2008.03.020>.
- [17] O.A. Golikova, Boron and Boron-based semiconductors, *Phys. Status Solidi* 51 (1) (1979) 11–40, <https://doi.org/10.1002/pssa.2210510102>.
- [18] I. Boustani, Systematic ab initio investigation of bare boron clusters: Determination of the geometry and electronic structures of (n=2-14), *Phys. Rev. B Condens. Matter* 55 (24) (1997) 16426–16438, <https://doi.org/10.1103/PhysRevB.55.16426>.
- [19] N. Vast, et al., Lattice dynamics of icosahedral α -boron under pressure, *Phys. Rev. Lett.* 78 (4) (1997) 693–696, <https://doi.org/10.1103/PhysRevLett.78.693>.
- [20] M. Fujimori, et al., Peculiar covalent bonds in α -rhombohedral boron, *Phys. Rev. Lett.* 82 (22) (1999) 4452–4455, <https://doi.org/10.1103/PhysRevLett.82.4452>.
- [21] I. Boustani, A comparative study of ab initio SCF-CI and DFT. Example of small boron clusters, *Chem. Phys. Lett.* 233 (3) (1995) 273–278, [https://doi.org/10.1016/0009-2614\(94\)01449-6](https://doi.org/10.1016/0009-2614(94)01449-6).
- [22] Ab Initio study B12 B13.pdf." .
- [23] R. Kawai, J.H. Weare, Instability of the B12 icosahedral cluster: rearrangement to a lower energy structure, *J. Chem. Phys.* 95 (2) (1991) 1151–1159, <https://doi.org/10.1063/1.461145>.

- [24] L. Hanley, J.L. Whitten, S.L. Anderson, Collision-induced dissociation and ab initio studies of boron cluster ions: determination of structures and stabilities, *J. Phys. Chem.* 92 (20) (1988) 5803–5812, <https://doi.org/10.1021/j100331a052>.
- [25] J.F. Jia, H.S. Wu, H.J. Jiao, Structure and stability of (BN)_n clusters, *Acta Chim. Sin.* 61 (5) (2003) 653–659, <https://doi.org/10.1007/bf02969511>.
- [26] A.N. Alexandrova, A.I. Boldyrev, H.J. Zhai, L.S. Wang, All-boron aromatic clusters as potential new inorganic ligands and building blocks in chemistry, *Coord. Chem. Rev.* 250 (21–22) (2006) 2811–2866, <https://doi.org/10.1016/j.ccr.2006.03.032>.
- [27] H.J. Zhai, C.Q. Miao, S.D. Li, L.S. Wang, On the analogy of B-BO and B-Au chemical bonding in B11O - and B10Au- Clusters, *J. Phys. Chem. A* 114 (46) (2010) 12155–12161, <https://doi.org/10.1021/jp108668t>.
- [28] B.B. Averkiev, L.M. Wang, W. Huang, L.S. Wang, A.I. Boldyrev, Experimental and theoretical investigations of CB8-: towards rational design of hypercoordinated planar chemical species, *Phys. Chem. Chem. Phys.* 11 (42) (2009) 9840, <https://doi.org/10.1039/b908973j>. –9849.
- [29] A.N. Alexandrova, A.I. Boldyrev, H.J. Zhai, L.S. Wang, Photoelectron spectroscopy and ab initio study of the doubly antiaromatic B 62- dianion in the LiB 6-cluster, *J. Chem. Phys.* 122 (5) (2005) 1–8, <https://doi.org/10.1063/1.1839575>.
- [30] H.J. Zhai, B. Kiran, J. Li, L.S. Wang, Hydrocarbon analogues of boron clusters planarity, aromaticity and antiaromaticity, *Nat. Mater.* (2003), <https://doi.org/10.1038/nmat1012>.
- [31] Z.A. Piazza, H.S. Hu, W.L. Li, Y.F. Zhao, J. Li, L.S. Wang, Planar hexagonal B 36 as a potential basis for extended single-atom layer boron sheets, *Nat. Commun.* 5 (2014), <https://doi.org/10.1038/ncomms4113>.
- [32] W.L. Li, et al., The B35 cluster with a double-hexagonal vacancy: a new and more flexible structural motif for borophene, *J. Am. Chem. Soc.* 136 (35) (2014) 12257–12260, <https://doi.org/10.1021/ja507235s>.
- [33] X.M. Luo, et al., B26-: the smallest planar boron cluster with a hexagonal vacancy and a complicated potential landscape, *Chem. Phys. Lett.* 683 (2017) 336–341, <https://doi.org/10.1016/j.cplett.2016.12.051>.
- [34] Q. Chen, et al., B33- and B34-: aromatic planar boron clusters with a hexagonal vacancy, *Eur. J. Inorg. Chem.* 2017 (38) (2017) 4546–4551, <https://doi.org/10.1002/ejic.201700573>.
- [35] Q. Chen, et al., Planar B38- and B37- clusters with a double-hexagonal vacancy: molecular motifs for borophenes, *Nanoscale* 9 (13) (2017) 4550–4557, <https://doi.org/10.1039/c7nr00641a>.
- [36] S. Chopra, T. Lu, A DFT/TDDFT and QTAIM based investigation of the titanium-doped Boron-38 cluster, *Theor. Chem. Acc.* 139 (8) (2020), <https://doi.org/10.1007/s00214-020-02647-3>.
- [37] C. Kim, T. Fujino, T. Hayashi, M. Endo, M.S. Dresselhaus, Structural and electrochemical properties of pristine and B-doped materials for the anode of Li-ion secondary batteries, *J. Electrochem. Soc.* 147 (4) (2000) 1265, <https://doi.org/10.1149/1.1393347>.
- [38] T. Jian, X. Chen, S.D. Li, A.I. Boldyrev, J. Li, L.S. Wang, Probing the structures and bonding of size-selected boron and doped-boron clusters, *Chem. Soc. Rev.* 48 (13) (2019) 3550–3591, <https://doi.org/10.1039/c9cs00233b>.
- [39] S. Xu, R. Dong, C. Lv, C. Wang, Y. Cui, Configurations and characteristics of boron and B36 clusters, *J. Mol. Model.* 23 (7) (2017), <https://doi.org/10.1007/s00894-017-3377-x>.
- [40] T. Nakayama, K. Kimura, Thermoelectric properties of boron-rich icosahedral cluster semiconductors, *Nippon Kinzoku Gakkaishi/J. Japan Inst. Met.* 63 (11) (1999) 1400–1406, https://doi.org/10.2320/jinstmet1952.63.11_1400.
- [41] W.L. Li, et al., The planar CoB18-Cluster as a motif for metallo-borophenes, *Angew. Chem - Int. Ed.* 55 (26) (2016) 7358–7363, <https://doi.org/10.1002/anie.201601548>.
- [42] B. Le Chen, et al., Structural stability and evolution of medium-sized tantalum-doped boron clusters: a half-sandwich-structured TaB12- cluster, *Inorg. Chem.* 57 (1) (2018) 343–350, <https://doi.org/10.1021/acs.inorgchem.7b02585>.
- [43] M. K. Hossain D. Roy Milon, F. Ahmed, Boron nanocluster as a heavy metal adsorbent in aqueous environment: a DFT Study, *J. Mol. Struct.* 1237 (April) (2021), 130302, <https://doi.org/10.1016/j.molstruc.2021.130302>.
- [44] S.U.D. Shamim, et al., A DFT study on the geometrical structures, electronic, and spectroscopic properties of inverse sandwich monocyclic boron nanoclusters ConBm (n = 1,2; m = 6–8), *J. Mol. Model.* 26 (6) (2020), <https://doi.org/10.1007/s00894-020-04419-z>.
- [45] M. Ren, et al., NbB12- a new member of half-sandwich type doped boron clusters with high stability, *Phys. Chem. Chem. Phys.* 21 (39) (2019) 21746–21752, <https://doi.org/10.1039/c9cp03496j>.
- [46] S. Azhagiri, S. Jayakumar, S. Gunasekaran, S. Srinivasan, Molecular structure, Mulliken charge, frontier molecular orbital and first hyperpolarizability analysis on 2-nitroaniline and 4-methoxy-2-nitroaniline using density functional theory, *Spectrochim. Acta Part A Mol. Biomol. Spectrosc.* (2014), <https://doi.org/10.1016/j.saa.2013.12.106>.
- [47] H.T. Pham, M.T. Nguyen, Effects of bimetallic doping on small cyclic and tubular boron clusters: B7M2 and B14M2 structures with M = Fe, Co, *Phys. Chem. Chem. Phys.* (2015), <https://doi.org/10.1039/c5cp01650a>.
- [48] J. Wang, L. Ma, Y. Liang, M. Gao, G. Wang, Density functional theory study of transition metals doped B80 fullerene, *J. Theor. Comput. Chem.* (2014), <https://doi.org/10.1142/S0219633614500503>.
- [49] M. Seeger, Gaussian processes for machine learning, *Int. J. Neural Syst.* (2004), <https://doi.org/10.1142/S0129065704001899>.
- [50] M.J. Frisch, et al., Gaussian 09, Revision B.01, Gaussian, Inc., Wallingford CT, 2009.
- [51] P. Fuentealba, H. Stoll, L. Von Szepenty, P. Schwerdtfeger, H. Preuss, On the reliability of semi-empirical pseudopotentials: simulation of Hartree-Fock and Dirac-fock results, *J. Phys. B Atom. Mol. Phys.* 16 (11) (1983), <https://doi.org/10.1088/0022-3700/16/11/001>.
- [52] W.R. Wadt, P.J. Hay, Ab initio effective core potentials for molecular calculations. Potentials for main group elements Na to Bi, *J. Chem. Phys.* 82 (1) (1985) 284–298, <https://doi.org/10.1063/1.448800>.
- [53] F.C. Tsai, C.C. Chang, C.L. Liu, W.C. Chen, S.A. Jenekhe, New thiophene-linked conjugated poly(azomethine)s: theoretical electronic structure, synthesis, and properties, *Macromolecules* 38 (5) (2005) 1958–1966, <https://doi.org/10.1021/ma048112o>.
- [54] E. Fabiano, F. Della Sala, R. Cingolani, Ab-initio study of singlet and triplet excitation energies in oligothiophenes, *Phys. Status Solidi C: Conferences* 1 (3) (2004) 539–542, <https://doi.org/10.1002/pssc.200304034>.
- [55] R. Bott, Gaussian 09, Igarss 2014 1 (2014) 1–5, <https://doi.org/10.1007/s13398-014-0173-7.2>.
- [56] A.S. Rad, S.S. Shabestari, S.A. Jafari, M.R. Zardoost, A. Mirabi, N-doped graphene as a nanostructure adsorbent for carbon monoxide: DFT calculations, *Mol. Phys.* (2016), <https://doi.org/10.1080/00268976.2016.1145748>.
- [57] T. Marwala, Gaussian mixture models, in: *Handbook of Machine Learning*, 2018.
- [58] R.G. Pearson, Absolute electronegativity and hardness: application to inorganic chemistry, *Inorg. Chem.* 27 (4) (1988) 734–740, <https://doi.org/10.1021/ic00277a030>.
- [59] G. Makov, Chemical hardness in density functional theory, *J. Phys. Chem.* 99 (23) (1995) 9337–9339, <https://doi.org/10.1021/j100023a006>.
- [60] X. Tu, H. Xu, C. Li, X. Liu, G. Fan, W. Sun, Adsorption performance of boron nitride nanomaterials as effective drug delivery carriers for anticancer drugs based on density functional theory, *Comp. Theor. Chem.* (2021), <https://doi.org/10.1016/j.comptc.2021.113360>.
- [61] N.O. Obi-Egbedi, I.B. Obot, M.I. El-Khaiary, Quantum chemical investigation and statistical analysis of the relationship between corrosion inhibition efficiency and molecular structure of xanthene and its derivatives on mild steel in sulphuric acid, *J. Mol. Struct.* (2011), <https://doi.org/10.1016/j.molstruc.2011.07.003>.
- [62] C.P. Smyth, Dipole moments, *Ind. Eng. Chem.* (1931), <https://doi.org/10.1021/ie50263a009>.
- [63] P.W. Tasker, The stability of ionic crystal surfaces, *J. Phys. C Solid State Phys.* (1979), <https://doi.org/10.1088/0022-3719/12/22/036>.
- [64] J. Pálinskás, A. Smola, Polarized light, in: *Mitochondrial Medicine: Mitochondrial Metabolism, Diseases, Diagnosis and Therapy*, 2008.
- [65] P. Arief, No Title37–39 (1995) 66 עליון הנושא "תחנות מצב", ענף הקיינוס תחנות מצב.
- [66] A. Dongre, P. Bhisey, U. Khopkar, Polarized light microscopy, *Indian J. Dermatol., Venereol. Leprol.* (2007), <https://doi.org/10.5334/bj>.
- [67] J.A. Klun, D. Ma, R. Gupta, Optically active arthropod repellents for use against disease vectors, *J. Med. Entomol.* 37 (1) (2000) 182–186, <https://doi.org/10.1603/0022-2585-37.1.182>.

- [68] T.H. Windhorn, C.A. Cain, Optically active binary liquid crystal thermometry, *IEEE Trans. Biomed. Eng.* 26 (3) (1979) 148–152, <https://doi.org/10.1109/TBME.1979.326473>. BME.
- [69] S. Grimme, Molecular electrostatic potentials: concepts and applications, *Z. Phys. Chem.* (1998), https://doi.org/10.1524/zpch.1998.205.part_1.136b.
- [70] F.A. Bulat, et al., Hydrogenation and fluorination of graphene models: analysis via the average local ionization energy, *J. Phys. Chem. A* (2012), <https://doi.org/10.1021/jp3053604>.
- [71] F.A. Bulat, A. Toro-Labbé, T. Brinck, J.S. Murray, P. Politzer, Quantitative Analysis of Molecular Surfaces: Areas, Volumes, Electrostatic Potentials and Average Local Ionization Energies, 2010, <https://doi.org/10.1007/s00894-010-0692-x>.
- [72] P. Wurfel, The chemical potential of radiation, *J. Phys. C Solid State Phys.* (1982), <https://doi.org/10.1088/0022-3719/15/18/012>.
- [73] X.E. Shen, X.Q. Shan, D.M. Dong, X.Y. Hua, G. Owens, Kinetics and thermodynamics of sorption of nitroaromatic compounds to as-grown and oxidized multiwalled carbon nanotubes, *J. Colloid Interface Sci.* 330 (1) (2009) 1–8, <https://doi.org/10.1016/j.jcis.2008.10.023>.
- [74] C.J.M. Chin, M.W. Shih, H.J. Tsai, Adsorption of nonpolar benzene derivatives on single-walled carbon nanotubes, *Appl. Surf. Sci.* 256 (20) (2010) 6035–6039, <https://doi.org/10.1016/j.apsusc.2010.03.115>.